1 *Revision 1*

2 "Growth dynamics of vaterite in relation to the physico-chemical properties of its

3 precursor, amorphous calcium carbonate, in the Ca–CO$_3$–PO$_4$ system"

4

5 Yuki Sugiura[1,2,3], Kazuo Onuma[2], and Atsushi Yamazaki[1]

6

7 *[1] School of National Resources and Environmental Science, Department of Creative*

8 *Science and Technology, Waseda University, 3-4-1, Okubo, Shinjuku-ku, Tokyo*

9 *169-8555,*

10 *Japan*

11 *[2] National Institute of Advanced Industrial Science and Technology, Central 6, 1-1-1,*

12 *Higashi, Tsukuba, Ibaragi 305-8566, Japan*

13 *[3] Department of Biomaterials, Faculty of Dental Science, Kyushu University, 3-1-1*

14 *Maidashi, Higashi, Fukuoka 812-0054, Japan*

15 Corresponding authors:

16 ysugiura@dent.kyushu-u.ac.jp (Y.S), +81-92-642-6346

17 FAX (Y.S): +81-92-642-6346

18

19

20   All authors approved the final manuscript.

21

22

23

24

25

26

27

28

29

30

31

32

33

34

35

36

37

38   **Abstract**

39   Vaterite is one of three non-hydrate calcium carbonate crystalline polymorphs and

40   is formed as an initial phase under pseudo-biological conditions. However, biological

41   hard tissues that use vaterite are rare; the reason for vaterite rarely appearing *in vivo* is

42   still unclear. There is consensus that, in phosphate-containing solutions, vaterite barely

43   forms and amorphous calcium carbonate (ACC), the precursor of crystalline calcium

44   carbonate and considered as aggregation of growth unit of vaterite, is stabilized. In this

45   study, to clarify the biomineralization process, we investigated how phosphate act as an

46   inhibitor of vaterite growth. We measured vaterite growth rates *in situ* and estimated the

47   essential crystal growth parameter, edge free energy, in the $Ca-CO_3-PO_4$ system in

48   relation to the physico-chemical properties of ACC. The effects of PO_4 on the ACC

49   structure and dynamics were also observed.

50   Co-existed PO_4 reduced the growth rate of vaterite even when it was added in μM

51   concentrations. The surface free energy of vaterite increased with increasing PO_4

52   concentration and was 10 times higher in a 10 μM PO_4-containing solution than in a

53   PO_4-free solution. Spectroscopic analyses showed that the chemical bonds in ACC

54   particles were drastically changed by the addition of μM scale PO_4, and the particles

55   could no longer transform into vaterite. We conclude that PO_4 inhibits vaterite growth

56   and changed the ACC structure. And the original growth units of vaterite were also

57   modified to the other structures. Thus, vaterite crystals could not grow by association of

58   these growth units, which resulted in an increase in the apparent surface free energy of

59   vaterite.

60

61   Key words: Vaterite, Crystal growth, intermediate phase, biomineralization

62

63

64

65

66

67

68

69

70

71

72

73

74

75 **INTRODUCTION**

76   Calcium carbonate minerals are the main component of hard tissues in

77 nonvertebrate animals such as mollusks, coral reefs and coccoliths (Deer et al., 1992;

78 Dove et al., 2003; Mann, 2005; Sunagawa, 2005). These minerals have three anhydrous

79 crystalline phases, calcite, aragonite and vaterite; two hydrated phases,

80 monohydrocalcite and ikaite; and amorphous phases (at least five phases), amorphous

81 calcium carbonates (ACC) (Deer et al., 1992; Kraji and Brecevic, 1995; Dove et al.,

82 2003; Mann, 2005; Sunagawa, 2005; Colfen and Antonietti, 2008; Gebauer et al., 2010,

83 Radha et al. 2010). These phases form as metabolic products in living creatures; this

84 process is known as biomineralization. Biomineralization normally occurs in weakly

85 basic aqueous solutions such as body fluids and seawater under normal temperature and

86 pressure, i.e., it is a relatively stable reaction and process (Deer et al., 1992; Dove et al.,

87 2003; Mann, 2005; Sunagawa, 2005). In addition, the numerous chemical species that

88 are present in organisms affect biomineralization (Deer et al., 1992; Dove et al., 2003;

89 Mann, 2005; Sunagawa, 2005; Bentov et al., 2010; Akiva-Tal et al., 2011; Sato et al.,

90 2011). The final products have various morphologies and crystal structures that are

91   suitable for biological applications.

92   The growth dynamics of calcium carbonate minerals, particularly in simulated

93   biological environments, has been a matter of great research interest in the field of

94   geochemistry and biomineralization (Sunagawa, 2005; Colfen and Antonietti, 2008;

95   Gebauer et al. 2008). Studies in this area may assist in clarifying complex biological

96   crystallization processes, and biological evolution, and the knowledge gained may be

97   used to generate new functional biomaterials.

98   Vaterite is not only an anhydrous crystalline polymorph of calcium carbonate and

99   an intermediate and metastable phase in weak basic solutions (Plummer and Busenberg,

100   1982; Brecevic and Nielsen, 1989; Deer et al., 1992; Sunagawa, 2005;

101   Rodriguez-Blanco et al., 2010) but also occurs as a biogenic mineral a component of

102   marine organisms, fish otoliths, and gastropod egg shells (Carlstrom, 1963; Hall and

103   Taylor, 1971; Lowenstam, 1975). It has a higher solubility and a comparatively lower

104   crystallinity than calcite and aragonite (Plummer and Busenberg, 1982; Sunagawa,

105   2005; Colfen and Antonietti, 2008). It occurs in various shapes, namely, irregular,

106   wire-like, and hexagonal because of crystallization with additives such as polymers and

107   NH_3- ions (Xu et al. 2005; Balz et al. 2006). Although vaterite was an initial crystalline

108   phase in weak basic solution, the growth mechanism of vaterite is unclear compared

109   with those of calcite and aragonite. Olderøy et al. (2009) estimated the growth rate of

110   vaterite spherulites in supersaturated solutions. They measured the seeded-vaterite

111   radius *ex situ* and the Ca concentration as a function of vaterite growth rate.

112   Gomez-Morales et al. (1996) and Kawano et al. (2009) estimated the surface free

113   energy of vaterite, which is a key parameter in growth, using the incubation time for

114   nucleation in various supersaturated solutions. However, these studies have provided

115   little conclusive information on the growth mechanism of vaterite because there has

116   been a consensus that vaterite crystals do not grow simply by attachment of ionic

117   species in aqueous solutions. Gebauer et al. (2008/2010), Pouget et al. (2009/2010), and

118   Demichelis et al. (2011) indicated that vaterite is formed via ACC, which is a random

119   aggregate of nanometer-scale essential clusters (called pre-nucleation clusters) that form

120   the vaterite structure through cluster-based structural transformation. Sugiura et al.

121   (2014) showed that a vaterite-like intermediate phase (called pseudo-vaterite) appeared

122   prior to vaterite nucleation in the presence of PO_4. This intermediate phase had a more

123   poor structure and a higher C/Ca ratio than those of vaterite, and greatly affected the

124   formation of vaterite. Thus, it is necessary to investigate the relationship between the

125   physico-chemical properties of ACC and the growth dynamics of pseudo-vaterite and

126   vaterite in relation to their structures. In addition, when we apply the growth model of

127   vaterite estimated *in vitro* to actual living organisms, we should consider the effect of

128   PO4 because it is universally present *in vivo*. Sugiura et al. (2013) showed that one of

129   the roles of PO_4 is a strong inhibition of vaterite transformation from ACC in simulated

130   biological conditions. They also reported that PO_4 is easily incorporated into ACC.

131   Taking into account these considerations, we provide here a new growth model of

132   vaterite from *in situ* optical microscopic observations in the $Ca–CO_3–PO_4$ system under

133   simulated biological temperature, pressure, and pH. In addition to vaterite growth rate,

134   we characterized ACC structures in relation to vaterite growth. We show that vaterite

135   only formed via transformation from an ACC phase, and PO_4 affected the chemical

136   bond structure between Ca and CO_3, thus forming a non-vaterite structure in ACC,

137   resulting in inhibition of vaterite nucleation and growth.

138

139   **EXPERIMENTAL METHODS**

140   **Solution preparation**

141        $CaCl_2$ and $NaHCO_3$ were purchased from Wako Pure Inc., Japan. NaCl, K_2HPO_4

142   and, KH_2PO_4 were purchased from Nakalai Tesque Inc., Japan. All reagents were

143   dissolved into ultra-pure water. We prepared seven mother solutions: 1 M $CaCl_2$ and

144   NaCl, 0.5 M $NaHCO_3$, K_2HPO_4 and KH_2PO_4, 25 mM NaCl and KH_2PO_4 solutions.

145

Measurement of vaterite spherulite growth rate and estimation of surface free

energy using direct Ca and CO$_3$ containing solution mixing and observation cell.

The details of the optical measurements and the surface free energy calculation

using the two-dimensional nucleation theory are described in Appendix. Briefly, a

growth cell for *in situ* observation of vaterite spherulite growth at various levels of

supersaturation was prepared. Owing to the higher solubility of vaterite than that of

calcite, it is difficult to maintain supersaturation with respect to vaterite during

experiments with a constant flow of supersaturated solution through the whole system.

Thus, we performed a rapid mixing system of a cation solution with an anion solution in

the observation cell to avoid undesirable homogeneous nucleation before introduction

of the solution into the cell.

Fig. 1a shows the schematic solution-flow system. The system consisted of two

solution pumps and silicone and Teflon○R tubes. Two pumps delivered the cation and

anion solutions separately into the observation cell, where the solutions were rapidly

mixed. It also enabled the introduction of the highly supersaturated solution into the

observation cell and enabled its ejection thereby avoiding homogeneous nucleation. Fig.

1b shows the schematic image of both mixing and observation cell. The cell was

163   composed of pieces of glass slide which induced heterogeneous nucleation and

164   polypropylene spacers. It enabled that fresh mixed supersaturated solutions were carried

165   into crystals heterogeneous nucleation and growth. The observation area was

166   approximately 100 μm thick, 1 mm wide and 7 mm long. The solution was disposed of

167   after passing the observation area, and fresh mixed solution was continuously supplied

168   to the area to maintain supersaturation with respect to precipitated vaterite. The flow

169   rates of cation and anion solutions were 2 mL/min, and the Reynolds number just after

170   the mixing was estimated to be about 4500 indicating that the two solutions were

171   completely mixed. The solution pH was maintained at about 8.6 by the buffering effect

172   of HCO_3^-.

173   The ionic activities of vaterite and pseudo-vaterite were given using Ca^{2+} and

174   CO_3^{2-} concentrations in the prepared solutions as

175          $I_{p(vaterite, pseudo-vaterite)} = [Ca^{2+}][CO_3^{2-}]$ (2)

176   The supersaturation ranges, σ in this study are 0.25–2.13 for vaterite and

177   0.16–1.89

178   for pseudo-vaterite. (see Resulting section and Appendix)

179

180   **Characterization of formed vaterite and pseudo-vaterite in supersaturated**

181   **solutions.**

182   The details are described in Appendix. In brief, the precipitated vaterite

183   spherulites, containing both vaterite and pseudo-vaterite, were characterized using

184   SAXS, EDX, and solid-state NMR.

185

186   **Characterization of ACC structure and dynamics.**

187   In addition to the vaterite spherulites growth experiments, we used Raman

188   spectroscopy to measure how ACC, a precursor phase of the vaterite structure, altered in

189   various PO_4-containing solutions. In addition, the PO_4 molar ratio (Ca/PO_4) of ACC

190   was measured using ICP-AES. The experiment details are described in Appendix.

191

192   **RESULTS**

193   **Growth behaviors and phase characterization of vaterite spherulites**

194   Our previous study (Sugiura et al. 2014) revealed that vaterite spherulites were

195   not a unique phase, but consisted of vaterite and pseudo-vaterite. The latter formed

196   before vaterite and had lower stability, higher solubility, poor crystallinity, and a higher

197   C/Ca ratio compared to those of vaterite. EDX and SAXS analyses can be used to

198   distinguish vaterite from pseudo-vaterite.

199   Figs. 2a show the same vaterite spherulite observed at different growth periods

200   using optical microscopy. The spherulite had a rounded morphology in the early stage

201   (20 s); however, the round shape was lost and became irregular over time (140 s). We

202   observed a decrease in the growth rate with time despite constant supersaturation (Fig.

203   2b). Furthermore, it displays very different physico-chemical properties from those of

204   the earlier formed rounded parts and the irregular shapes that formed on those rounded

205   parts (see Fig. 3 and Fig. S1 and S2).

206   The rounded spherulite morphology observed during the period of faster growth

207   rate also changed and became irregular after the growth rate became slower. The

208   FE-SEM images showed that the rounded vaterite spherulites comprised many sub 100

209   nm scale particles as has been demonstrated in previous studies (Pouget et al.

210   2009/2010; Rodriguez-Blanco et al. 2011). Irregularly shaped spherulites (Fig. 3a)

211   changed to a hollow-shell structure irrespective of the presence of PO_4 (Fig. 3b) after

212   washed several times with 10 mM $NaHCO_3$ solution. FE-SEM/EDX measurements

213   showed that the average C/Ca ratio of the outer regions of the shell (the part of irregular

214   shape) was 1.03 and that of the inner regions of the shell was 1.28 (Table 1).

215   The SAXS measurements for irregularly shaped spherulites showed a bi-modal

216   crystallite size distribution with peaks at approximately 5 nm and at 50–200 nm.

217   However, the peak at 5 nm became weak for washed hollow-structure vaterite, and the

218   size distribution changed to almost unimodal with a peak at 50–200 nm (Fig. 3c). The

219   law data for the SAXS-XRD pattern is in Appendix (Fig. S1).

220   The solid state NMR (^{31}P and ^{13}C MAS spectra) for rounded vaterite and hollow

221   structural vaterite spherulites showed clear differences. This indicates that the

222   incorporation of PO_4 into vaterite and pseudo-vaterite structures is distinctly different

223   (see Fig. S2).

224

225   **Variation in surface free energy with PO$_4$ concentration**

226   We assumed that the chemical formula of vaterite or pseudo-vaterite was

227   stoichiometric, $CaCO_3$. The measured solubilities from the Ca concentrations were

228        $K_{sp(vaterite)} = [Ca^{2+}][CO_3^{2-}] = 1.04 \times 10^{-8}$ $[M/L]^2$ (2)

229   for vaterite and

230        $K_{sp(pseudo-vaterite)} = [Ca^{2+}][CO_3^{2-}] = 1.44 \times 10^{-8}$ $[M/L]^2$ (3)

231   for pseudo-vaterite, in our experimental conditions for ionic strength of 0.1 $[M/L]^2$

232   which values were similar to values of Plummer and Busenberg 1982 and lower than

233   that of ACC (2.9×10^{-8} $[M/L]^2$ calculated from Brecevic and Nielsen 1989).

234   Figs. 4a and b show R values for vaterite and pseudo-vaterite depending on σ in

235   PO_4 solutions. We measured R for each condition in more than 50 samples; the data

236   were averaged and standard deviations were calculated. The maximum error of R was

237   less than 25%.

238   R exponentially increased with increasing σ. With increasing PO_4 concentration,

239   on the other hand, R decreased even when σ was kept constant. At low values of σ (in a

240   PO_4-free solution, σ was 0.16 for pseudo-vaterite and 0.25 for vaterite, respectively) and

241   higher PO_4, nucleation of spherulites or growth of spherulite seeds was not detected,

242   despite observation for more than 3 h.

243   Using the relationship between R and σ, we calculated γ for two-dimensional

244   islands nucleated on vaterite or pseudo-vaterite in the PO_4 solutions. Fig. 5a shows the

245   relationship between $1/ln(1 + \sigma)$ and $ln\{R/\sigma^{2/3}(1 + \sigma)^{1/3}\{ln(1 + \sigma)\}^{1/6}\}$. A change in slope

246   was observed for $1/ln(1 + \sigma)$ greater than 1.8 for pseudo-vaterite and greater than 1.5 for

247   vaterite. As has been previously reported for several crystals that grow via a two

248   dimensional mode (Malkin et al., 1989; Onuma et al., 2000), we assumed that growth

249   proceeded via homogeneous nucleation for $1/ln(1 + \sigma)$ less than 1.8 and via

250   heterogeneous nucleation for $1/ln(1 + \sigma)$ greater than 1.8. The apparent γ values were

251   calculated using the plot in heterogeneous nucleation region. (Onuma et al., 1998). The

252   apparent γ values calculated for the homogeneous nucleation region were $2.43k_BT$ for

253   vaterite and $1.89k_BT$ for pseudo-vaterite in PO_4-free solutions.

254   The apparent γ values increased with increasing PO_4 concentration. However,

255   apparent γ for pseudo-vaterite was lower than that for vaterite at all concentration of

256   PO_4. We calculated the surface free energy, ΔG, of vaterite and pseudo-vaterite using

257   apparent γ. Fig. 5b shows the relationship between ΔG and PO_4 concentration. The ΔG

258   values in PO_4-free solutions were 30.7 mJ/m^2 for vaterite and 23.9 mJ/m^2 for

259   pseudo-vaterite, respectively. Gomez-Morales et al. (1996) reported $\Delta G = 40$ mJ/m^2 for

260   vaterite using the relationship between incubation time for three-dimensional nucleation

261   versus σ. Lakshtanov et al. (2010) also reported $\Delta G = 42$ mJ/m^2 for vaterite. Our results

262   are close

263   to this value. Furthermore, the value was smaller than that of calcite (48.5 mJ/m^2)

264   (Bruno

265   et al. 2013).

266   The value of ΔG increased with increasing PO_4 concentration; the rate of increase

267   for vaterite was higher than that for pseudo-vaterite. The ΔG values were 223.9 mJ/m^2

268   for vaterite and 105.2 mJ/m^2 for pseudo-vaterite in solutions with 10 μM PO_4 (Fig. 5b).

269   We applied growth models other than two-dimensional nucleation, spiral growth

270   and adhesive growth models (Ookawa, 1977; Saito, 2002), to analyze the growth rate

271 data because we could not observe the surfaces of the crystals directly. Both growth

272 models were inadequate because the calculated growth parameters and growth behavior

273 using both growth models showed clearly strange value (see details in Appendix).

274

275 **Dynamics and structures of ACC particles in Ca–CO$_3$–PO$_4$ system**

276 Fig. 6 shows the PO$_4$/Ca ratio of ACC formed immediately after solution

277 preparation in the presence of PO$_4$. The ratio increased linearly with increasing PO$_4$

278 concentration. The ratio was 3.8×10^{-3} in 20 μM PO$_4$ and 9.7×10^{-3} in 50 μM PO$_4$ both of

279 which contained 12.5 mM CaCO$_3$.

280 The ACC structure were also altered with increasing PO$_4$ content using Raman

281 spectroscopy. The details were described in Appendix. Briefly, as PO$_4$ concentration

282 increasing, ACC structures were altered calcite-like to vaterite-like.

283

284 **Discussions**

285 Calcium carbonate crystalline particles precipitated on the walls and at the bottom

286 of cells. In low-concentration PO$_4$ solutions, they mainly consisted of vaterite

287 spherulites, and the amount of calcite increased with increasing in PO$_4$ concentration.

288 Our study revealed the characteristics of vaterite growth dynamics in the

289     $Ca–CO_3–PO_4$ system under simulated biological conditions. In PO_4-free solutions, the

290   values for apparent edge free energy were $\gamma = 2.43k_BT$ for vaterite and $\gamma = 1.89k_BT$ for

291   pseudo-vaterite. Malkin et al. (1989) investigated the growth dynamics of the (101) face

292   of ammonium dihydrogen phosphate (ADP) crystal, which is a representative soluble

293   inorganic crystal. The (101) face grew by two-dimensional nucleation and γ was

294   estimated to be $0.7k_BT$. Sazaki et al. (1996) investigated the (101) face of the lysozyme

295   crystal of a protein crystal, and found that $\gamma = 2.8k_BT$. These studies indicate that the

296   value of γ greatly depends on the size of the essential growth unit of crystals, i.e.,

297   whether a crystal is an ionic species or a macroscopic molecule. The apparent value of γ

298   for vaterite and pseudo-vaterite was two or three times larger than that for soluble

299   inorganic crystals; this value was comparable with that for protein crystals and

300   hydroxyapatite. These growth units are considered as cluster- sized molecules (nm sized

301   particles) (Onuma and Ito 1998). The large γ of vaterite and pseudo-vaterite is

302   consistent with that of the previous studies on the growth unit of calcium carbonates, i.e.,

303   they are clusters.

304   Next, we discuss the inhibiting effect of PO_4 on vaterite growth. On the basis of

305   the growth rate measurements, there are two possibilities for the mechanism causing the

306   PO_4 effect. First, PO_4 is simply adsorbed onto the surface of vaterite and stops vaterite

307 growth. Second, PO_4 changes the ACC structure and inhibits its transformation into

308 vaterite. Gebauer et al. (2008/2010) and Demichelis et al. 2011 indicated that ACC is a

309 precursor of vaterite and suggested that ACC was an aggregate of the growth unit of

310 vaterite under weak basic solutions. In addition, our previous study (Sugiura et al. 2013)

311 showed that a small amount of PO_4 (PO_4/Ca ~1/1000) altered later calcium carbonate

312 crystalline phases, such as vaterite to calcite. Furthermore, the dynamics of ACC are

313 also significantly altered as PO_4 concentration increases.

314   Raman spectra indicated that the structure of ACC changed from calcite-like

315 amorphous into vaterite-like amorphous with an increase in PO_4 concentration.

316 However, they could not be transformed into crystalline vaterite. We assume that the

317 increase in vaterite-like structures in ACC with PO_4 did not correspond to *actual*

318 *vaterite structure*. These vaterite-like structures are assumed as "junk parts," and it is

319 suggested that their increase resulted in a marked reduction in the actual vaterite growth

320 rate. The ICP-AES measurement showed that PO_4 was easily incorporated into ACC

321 and altered its structure. The resulting physico-chemical properties from the

322 incorporation of Mg^{2+} ions and polymers into ACC have also been studied (Cheng et al.

323 2007; Oaki et al. 2008; Jiang et al. 2010). It suggests that ACC formed in relatively low

324 PO_4 concentration solutions are one of precursors in the formation of vaterite and

325   pseudo-vaterite. Thus, it is indicated that PO_4-ACC no longer acts as a growth unit of

326   vaterite and pseudo-vaterite.

327   Gebauer et al. (2008/2010) and Demichelis et al. (2011) investigated the structure

328   of pre-nucleation clusters of calcium carbonate under various pH conditions. They

329   showed that the size, distribution, and coordination number of the cluster increased with

330   an increase in solution pH. The essential chemical bond between Ca and CO_3 in ACC is

331   Ca–C, corresponding to a calcite-like structure at lower pH condition about 8.5, which

332   is comparable to our experimental condition, and O–Ca, corresponding to a vaterite-like

333   structure, at higher pH condition about 11.5. This conclusion was also supported by

334   experiments (Nebel et al., 2008). At lower pH, HCO_3^- ion pairs are formed in which H^+

335   bonds O of CO_3. This inhibits the formation of O–Ca bonds, resulting in ACC particles

336   with small particle distributions. They also indicated that the average size of ACC

337   particles increases at higher pH because of the absence of H^+ ions, which acts to block

338   ACC aggregation.

339   Our conclusion concerning the effect of PO4 on ACC structure is comparable to

340   that caused by increasing the pH of the solutions. When the results obtained by

341   Demichelis et al. (2011) are applied to this case, it appears that PO4 (probably the

342   HPO_4^{2-} form) binds H^+ in ACC and changes the ACC structure. This drastically reduces

343 the number of growth units that originally construct the vaterite structure via

344 cluster-based phase transformation from ACC. Some previous studies had investigated

345 the effect of H^+ on amorphous phases (Wang et al., 2009; Sugiura et al., 2011), and they

346 support these conclusion.

347   The effect of PO_4 on vaterite growth can be summarized as follows. PO_4 is not

348 only absorbed on the surface of vaterite as a conventional impurity but also changes the

349 structure of the growth unit in ACC *before* the vaterite forms via phase transformation

350 from ACC. This modified structure is vaterite-like, but is never the actual vaterite

351 structure.

352   Although supersaturation of the solution is defined using the $CaCO_3$

353 concentration, where PO_4 ions co-existed they reduced the growth units of vaterite; it is

354 observed that vaterite grew through cluster-based crystal growth. For this reason,

355 despite the average Ca-CO_3 ion concentration being kept constant, the actual

356 supersaturation rate decreased as the PO_4 concentration increased. Because of this

357 decrease in actual supersaturation (from the retardation of vaterite growth by PO_4 ions)

358 a higher supersaturation of the bulk solution than would be expected was required for

359 the nucleation and growth of vaterite. Consequently, this causes an increase in the

360 apparent surface energy of vaterite in PO_4^- containing solutions.

361   Because of the difference in apparent surface free energy, pseudo-vaterite phase is

362   likely to precipitate under high PO_4 concentrations. When the PO_4 concentration further

363   increases, crystalline vaterite dose not precipitate, and ACC with a vaterite-like

364   chemical structure is stable.

365   We obtained conclusive information in this study to explain why vaterite is rarely

366   observed in biological hard tissues. Small amounts of PO_4 ($PO_4/CaCO_3$ = ~1/1000),

367   which is essential for all living organisms, are sufficient to inhibit vaterite nucleation

368   and growth. We also observed that fluctuations in PO4 concentration caused the

369   formation of nonuniform vaterite-like structures, which are inadequate for stable hard

370   tissues *in vivo*.

371

372   **Implications**

373   We investigated the growth dynamics of vaterite and pseudo-vaterite in the

374   Ca-CO$_3$–PO$_4$ system under simulated biological conditions in relation to the

375   physicochemical properties of ACC, the precursor of vaterite. A possible inhibition

376   mechanism of PO_4 on vaterite growth is that the apparent surface free energy was

377   increased by decreasing supersaturation with respect to vaterite, which is caused by the

378   reduction of cluster numbers corresponding to vaterite structure in ACC. This effect is

379   more evident in vaterite than in pseudo-vaterite because the structure of

380   pseudo-vaterite is looser than that of vaterite. Therefore, in higher PO_4 solutions, the

381   unstable phase of pseudo-vaterite is likely to appear instead of vaterite because of its

382   lower surface free energy in the early stages of calcium carbonate formation.

383   With an increase in PO_4 concentration, the dominant phase in the solution

384   changes to a more unstable form of vaterite. Furthermore, it is suggested that unstable

385   vaterite phases formed in high PO_4 solutions easily convert calcite through dissolution

386   and precipitation because their physico-chemical properties are highly unstable

387   compared with conventional vaterite (Sugiura et al. 2013).

388   This suggestion of how PO_4 affects vaterite formation processes relating to its

389   precursor ACC contributes not only to biomineralization process investigation but also

390   suggests that calcium carbonate polymorphism by other biocompatible elements such

391   as Mg^{2+} and SO_4 is a possibility.

392

393

394

395

396

397

398

399

400

401

402

403

404

405

ACKNOWLEDGMENTS

415

416

417

418

419

420

421

422

423

REFERENCES CITES

425   Akiva-Tal A., Kababya S., Balazs Y. S., Glazer L., Berman A., Sagi A. and

426 Schmidt A. (2011) *In situ* molecular NMR picture of bioavailable calcium stabilized as

427 amorphous $CaCO_3$ biomineral in crayfish gastroliths. Proceedings of the National

428 Academy of Science of USA, 108, 14763-14768.

429   Balz M., Therese H. A., Li J., Gutmann J. S., Kappl M., Nasdala L., Hofmeister W.,

430 Butt H.-J., Tremel W. (2005) Crystallization of Vaterite Nanowires by the Cooperative

431 Interaction of Tailor-Made Nucleation Surfaces and Polyelectrolytes. Advanced

432 Functional Materials, 15, 683-688.

433   Bentov S., Weil S., Glazer L., Sagi, A. and Berman, A. (2010) Stabilization of

434   amorphous calcium carbonate by phosphate rich organic matrix proteins and by single

435   phosphoamino acids. Journal of Structural Biology, 171, 207-215.

436   Brecevic L. and Nielsen A. E. (1989) Solubility of amorphous calcium carbonate.

437   Journal of Crystal Growth, 98, 504-510.

438   Bruno M., Massaro F. R., Pastero L., Costa E., Rubbo M., Prencipe M. and

439   Aquilano D. (2013) New Estimates of the Free Energy of Calcite/Water Interfaces for

440   Evaluating the Equilibrium Shape and Nucleation Mechanisms. Crystal Growth and

441   Design, 13, 1170-1179.

442   Carlstrom D. (1963) A crystallographic study of vertebrate otoliths. Biological

443   Bulletin, 125, 124-128.

444   Cheng X. G., Varona P. L., Olszta M. J., Gower L. B. (2007) Biomimetic synthesis

445   of calcite films by a polymer-induced liquid-precursor (PILP) process 1. Influence and

446   incorporation of magnesium. Journal of Crystal Growth 307, 395-404.

447   Colfen H. and Antonietti M. (2008) Mesocrystals and Nonclassical Crystallization;

448   John Wiley and Sons Ltd., England.

449   Deer W. A., Howie R. A. and Zussman, J. (1992) An Introduction to the

450   Rock-Forming Minerals 2nd Edition; Pearson Education Ltd., UK.

451   Demichelis R., Raiteri P., Gale J. D., Quigley D. and Gebauer D. (2011) Stable

452   prenucleation mineral clusters are liquid-like ionic polymers. Nature Communications,

453   2,

454   590-597.

455   Demichelis R., Raiteri P., Gale J. D. and Dovesi R. (2013) The multiple structure

456   of vaterite. Crystal Growth and Design, 13, 2247-2251.

457   Dove P., DeYoreo J. J. and Weiner S. (2003) Reviews in Mineralogy and

458   Geochemistry, Vol. 54: Biomineralization. Mineralogical Society of America,

459   Geochemical Society, USA.

460   Gebauer D., Gunawidjaja P. N., Ko P. J. Y., Bacsik Z., Aziz B., Liu L., Hu Y.,

461   Bergstrom L., Tai C. W., Sham T. K., Eden M. and Hedin N. (2010) Proto-Calcite and

462   Proto-Vaterite in Amorphous Calcium Carbonates. Angewande Chemie International

463   Edition, 49, 8889–8891.

464   Gebauer D., Volkel A. and Colfen H. (2008) Stable pre-nucleation clusters for

465   calcium carbonate. Science, 322, 1819–1822.

466   Gomez-Morales J., Torrent-Burgues J. and Rodriguez-Clemente R. (1996)

467   Nucleation of calcium carbonate at different initial pH conditions. Journal of Crystal

468   Growth, 169, 331-338.

469   Greenwald I. (1945) The effect of phosphate on the solubility of calcium carbonate

470   and of bicarbonate on the solubility of calcium and magnesium phosphates. Journal of

471   Biological Chemistry, 161, 697-704.

472   Hall A., and Taylor J. D. (1971) The occurrence of vaterite in gastropod egg-shells.

473   Mineralogical Magazine, 38, 522-525.

474   Jiang J., Gao M. R., Qiu Y. H., Yu S. H. (2010) Gram-scale, low cost, rapid

475   synthesis of highly stable Mg-ACC nanoparticles and their long-term preservation.

476   Nanoscale, 2, 2358-2361.

477   Kawano J., Shimobayashi N., Miyake A. and Kitamura M. (2009) Precipitation

478   diagram of calcium carbonate polymorphs: its construction *and* significance. Journal of

479   Physics; Condensed. Matter, 21, 425102-425109.

480   Kraji D. and Brecevic L. (1995) Dissolution kinetics and solubility of calcium

481   carbonate monohydrate. Colloidal Surface A, 96, 287–293.

482   Lakshtanov L. Z. and Stipp S. L. S. Interaction between dissolved silica and

483   calcium carbonate: 1. Spontaneous precipitation of calcium carbonate in the presence of

484   dissolved silica. Geochimica et. Cosmochimica Acta, 74, 2655-2664.

485   Lowenstam H. A. and Abbott D. P. (1975) Vaterite: a mineralization product of the

486   hard tissues of a marine organism (Ascidiacea). Science, 188, 363-365. Malkin A. I.,

487 Chernov A. A. and Alexeev L.V. (1989) Growth of dipyramidal face of dislocation-free

488 ADP crystals; free energy of steps. Journal of Crystal Growth, 97, 765-769.

489 Mann S. (2005) Biomineralization, Principles and Concepts in Bioinorganic

490 Materials Chemistry. Oxford University Press, USA.

491 Nebel H., Neumann M., Mayer C. and Epple M. (2008) On the structure of

492 amorphous calcium carbonate–A detailed study by solid-state NMR spectroscopy.

493 Inorganic Chemistry, 47, 7874-7879.

494 Oaki Y., Kajiyama S., Nishimura T., Imai H., Kato T. (2008) Nanosegregated

495 amorphous composites of calcium carbonate and an organic polymer. Advanced

496 Materials 20, 3633-3637.

497 Olderøy M. Ø., Xie M., Strand B. L., Flaten E. M., Sikorski P. and Andreassen J. P.

498 (2009) Growth and nucleation of calcium carbonate vaterite crystals in presence of

499 alginate. Crystal Growth and Design, **9**, 5176-5183

500 Onuma K. and Ito A. (1998) Cluster growth model for hydroxyapatite. Chemistry

501 of Materials, 10, 3346-3351.

502 Onuma K., Ito A. and Tateishi T. (1996) Investigation of a growth unit of

503 hydroxyapatite crystal from the measurements of step kinetics. Journal of Crystal

504 Growth, 167, 773-776.

505   Onuma K., Kanzaki N., Ito A. and Tateishi T. (1998) Growth kinetics of the

506   hydroxyapatite (0001) face revealed by phase shift interferometry and atomic force

507   microscopy. Journal of Physical Chemistry B, 102, 7833-7838.

508   Plummer L. N. and Busenberg E. (1982) The solubilities of calcite, aragonite and

509   vaterite in CO_2-H_2O solutions between 0 and 90°C, and an evaluation of the aqueous

510   model for the system Ca–CO_3–H_2O. Geochimica et Cosmochimica Acta, 46,

511   1011-1040.

512   Pouget E. M., Bomans P. H. H., Goos J. A. C. M., Frederik P. M., de With G. and

513   Sommerdijk N. A. J. M. (2009) The initial stages of template-controlled $CaCO_3$

514   formation

515   revealed by cryo-TEM. Science, 323, 1455-1458.

516   Pouget E. M., Bomans P. H. H., Dey A., Frederik P. M., deWith G. and

517   Sommerdijk N. A. J. M. (2010) The Development of Morphology and Structure in

518   Hexagonal Vaterite. Journal of American Chemical Societies, 132, 11560-11565.

519   Posner A. S. and Betts F. (1975) Synthetic amorphous calcium phosphate and its

520   relation to bone mineral structure. Accounts of Chemical Research, 8, 273-281.

521   Radha A. V., Forbes T. Z., Killian C. E., Gilbert P. U. P. A. and Navrotsky A. (2010)

522   Transformation and crystallization energetic of synthetic and biogenic amorphous

523   calcium carbonate. Proceeding of National Academy of Science of USA, 107,

524   16438-16443.

525   Rodriguez-Blanco J. D., Shaw S. and Benning L. G. (2010) The kinetics and

526   mechanisms of amorphous calcium carbonate (ACC)crystallization to calcite, *via*

527   vaterite. Nanoscale, 3, 265–271.

528   Saito Y. (2002) Chapter 5: Surface kinetics. Crystal growth. Syokabo Co., Japan.

529   pp. 81-90. (in Japanese)

530   Sato A., Nagasaka S., Furihata K., Nagata S., Arai I., Saruwatari K., Kogure T.,

531   Sakuda S. and Nagasawa H. (2011) Glycolytic intermediates induce amorphous calcium

532   carbonate formation in crustaceans. Nature Chemical Biology, 7, 197–199.

533   Sazaki G., Kurihara K., Miyashita S., Komatsu H. and Nakada, T. (1996) *In situ*

534   observation of the concentration distribution around a lysozyme crystal by two-beam

535   interferometry. Journal of Japan Association of Cryst. Growth, 23, 413-421. (in

536   Japanese)

537   Sugiura Y., Onuma K., Kimura Y., Miura H. and Tsukamoto K. (2011)

538   Morphological evolution of precipitates during transformation of amorphous calcium

539   phosphate into octacalcium phosphate in relation to role of intermediate phase. Journal

540   of Crystal Growth, 332, 58-67.

541   Sugiura Y., Onuma K., Kimura Y., Tsukamoto K. and Yamazaki A. (2013)

542   Acceleration and inhibition effects of phosphate on phase transformation of amorphous

543   calcium carbonate into vaterite. American Mineralogist, 98, 262-270.

544   Sugiura Y., Onuma K., Nagao M., Momma K., Kimura Y. and Yamazaki A.

545   (2014) Dissolution behavior of vaterite spherulite in solutions containing phosphate ions.

546   Journal of the Ceramic Society of Japan, 122, 679-687.

547   Sunagawa I. (2005) Crystals-Growth, Morphology and Perfection. Cambridge

548   University Press, UK.

549   Tsuji T., Onuma K., Yamamoto A., Iijima M. and Shiba K. (2008) Direct

550   transformation from amorphous to crystalline calcium phosphate facilitated by

551   motif-programmed artificial proteins. Proceedings of National Academy Science of

552   USA, 105, 16866-16870.

553   Wang C. G., Liao J. W., Gou B. D., Huang J., Tang R. K., Tao J. H., Zhang T. L.

554   and Wang K. (2009) Crystallization at multiple sites inside particles of amorphous

555   calcium phosphate. Crystal Growth and Design, 9, 2620-2626.

556   Xu A.-W., Antonietti M., Colfen H., Fang Y.-P. (2006) Uniform Hexagonal Plates

557   of Vaterite $CaCO_3$ Mesocrystals Formed by Biomimetic Mineralization. Advanced

558   Functional Materials, 16, 903-908.

559

560

561

562

563

564

565

566

567

568

569

570

571

572   Figure Captions

573   Fig. 1. Experimental setup for vaterite growth rate measurement. (**a**) Overall diagram of

574   the observation system. The arrows indicate the flow direction of the solutions. (**b**)

575   Schematic of the growth cell. The cell consists of three parts: the solution mixing part,

576   the observation part, and the waste part. The circles indicate vaterite spherulites, the

577   rectangular area containing circles denotes the observation part, and the arrows indicate

578   the flow direction of the solutions.

579

580   Fig. 2. Growth behavior of precipitated spherulites in supersaturated solutions. (**a**)

581   Optical microscopic photograph of spherulites 20 s and 140 s after the start of growth.

582   Supersaturation σ was 1.80 for vaterite and 1.58 for pseudo-vaterite (PO$_4$-free

583   condition). The spherulites exhibit a well-rounded morphology. (**b**) Change in average

584   spherulite radius over time measured around at center of spherulites. Growth rate (slope

585   of line) of spherulites decreased after 60 s. The black dotted line corresponds to the

586   growth rate of pseudo-vaterite and the grey dotted line to that of vaterite.

587

588   Fig. 3. Phase characterization of spherulites. (**a**) FE-SEM photograph of irregularly

589   shaped spherulites precipitated in the same solution as Fig. 2. The photograph was taken

590   300 s after the start of growth. (**b**) FE-SEM photograph of hollow spherulites obtained

591   by washing the spherulites in (**a**) using 10 mM NaHCO$_3$ solution. (**c**) SAXS

592   measurements for (**a**) and (**b**). The crystallite probability of (**a**) and (**b**) is indicated

593   respectively.

594

595   Fig. 4. Relationship between R and σ in PO_4-containing solutions. (**a**) Pseudo-vaterite.

596   (**b**) Vaterite. The symbols and lines correspond to data measured at various PO_4

597   concentrations: grey solid diamonds with fine broken line (PO_4-free solution), grey

598   solid squares with fine broken line (1.25 μM PO_4-containing solution), grey solid circles

599   with fine broken line (2.50 μM PO_4-containing solution), black open diamonds with fine

600   broken line (5.00 μM PO_4-containing solution), grey open squares with fine broken line

601   (6.25 μM PO_4-containing solution), grey open circles with fine broken line (7.50 μM

602   PO_4-containing solution), grey solid diamonds with roughly broken line (8.75 μM

603   PO_4-containing solution) and grey solid squares with roughly broken line (10.00 μM

604   PO_4-containing solution).

605

606   Fig. 5. (**a**) Logarithmic plots of growth rate of the vaterite (solid circles) and

607   pseudo-vaterite (solid circles) for calculation of edge free energy under PO_4 free

608   conditions. (**b**) Change in surface free energies of vaterite (solid circles with dotted line)

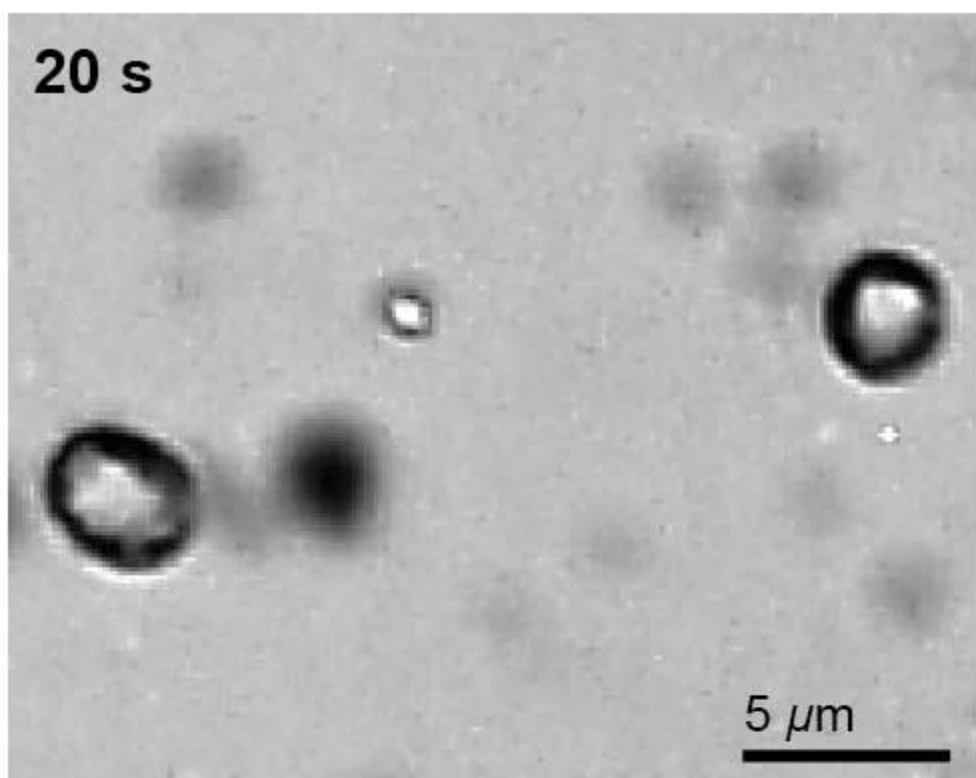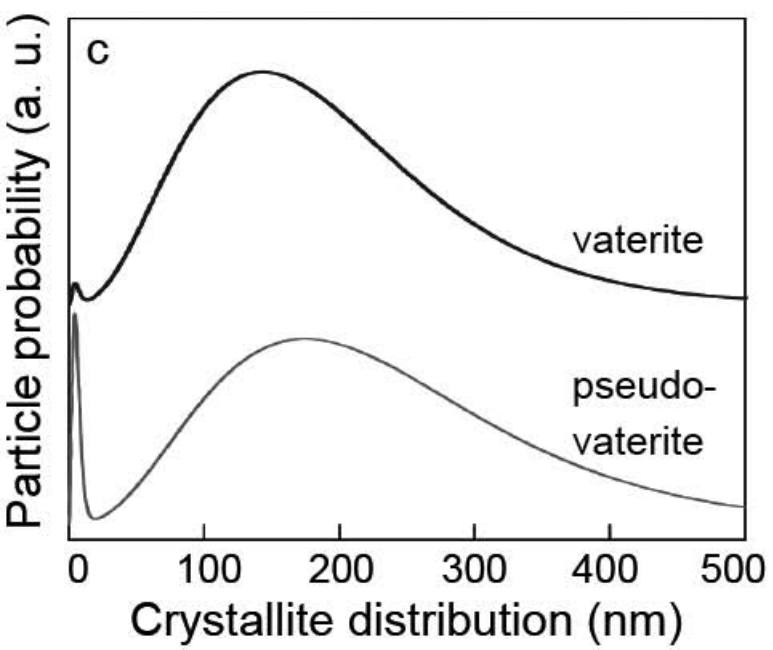609   and pseudo-vaterite (solid diamonds with dotted line) with PO_4 concentration.
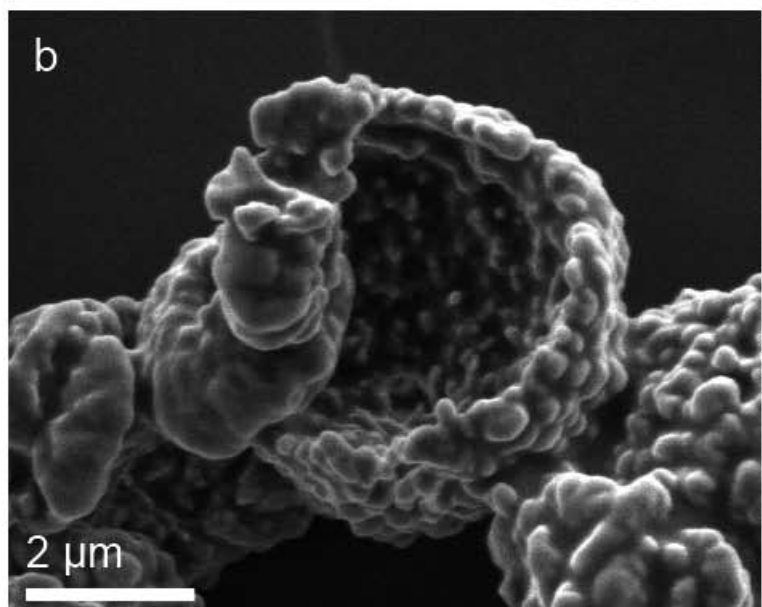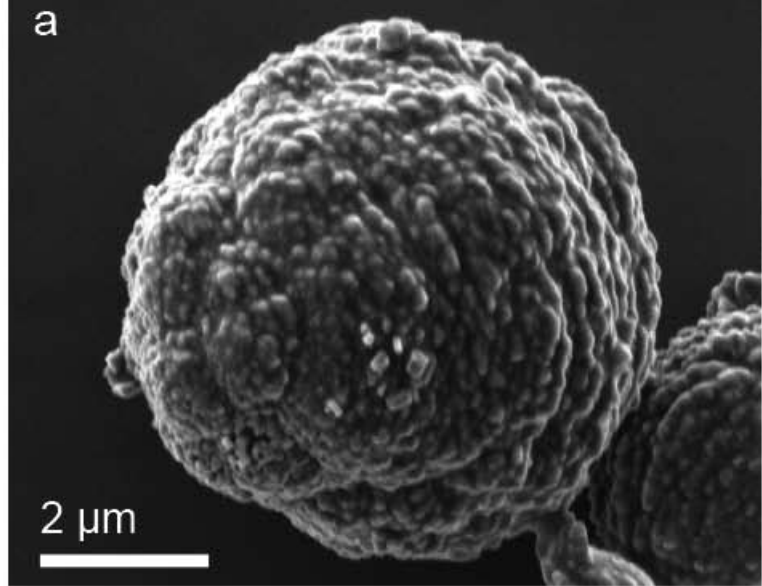
610

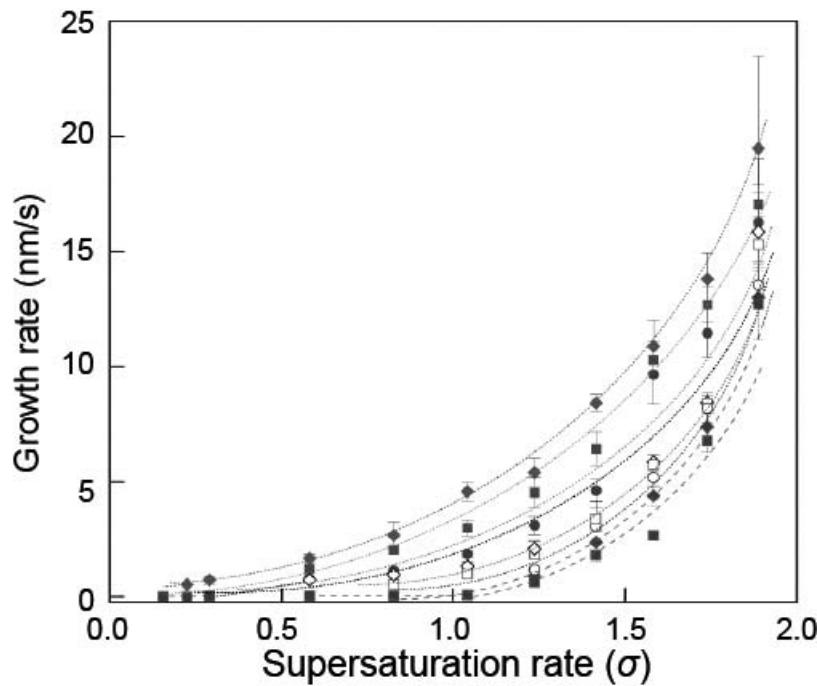611   Fig. 6. PO_4/Ca ratio of ACC precipitated in PO_4-containing solutions.

612

613   Table 1. Summary of the physico-chemical properties of vaterite and pseudo-vaterite in

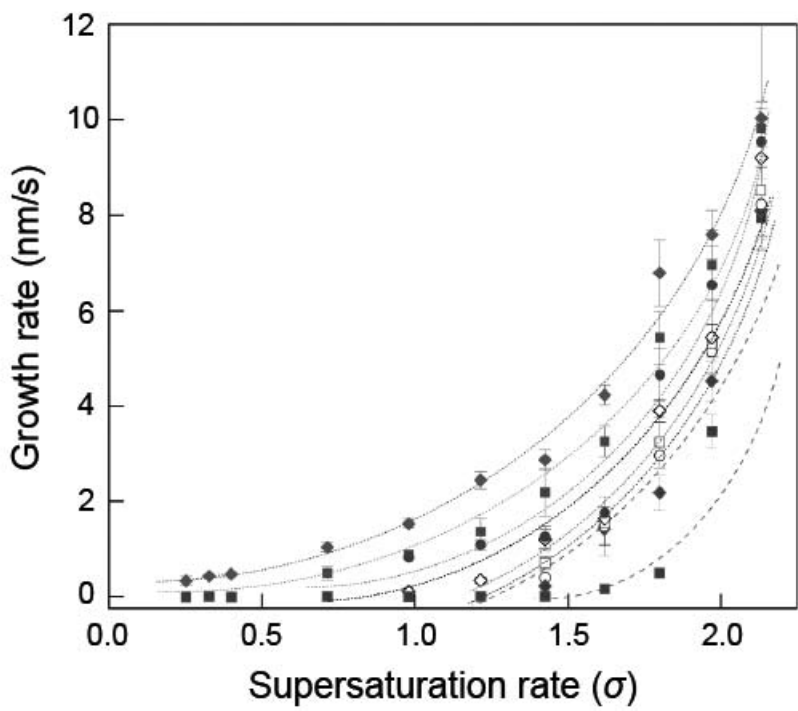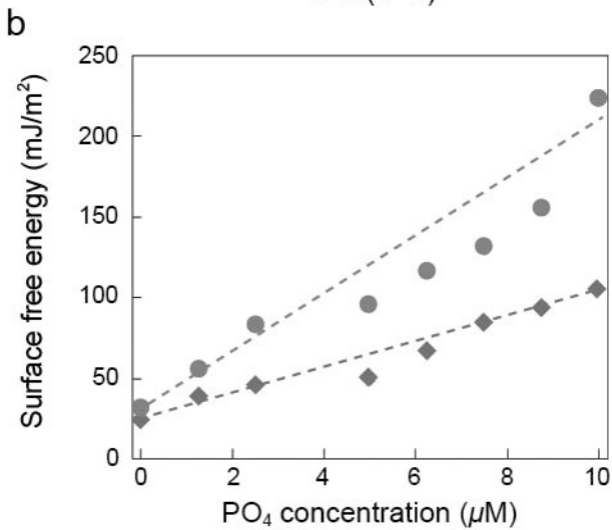614   the Ca–CO$_3$–PO$_4$ system.

a

b

5 mm

a

20 s

5 μm

140 s

5 μm

b

a

b

a

$\ln\{R/\sigma^{2/3}(1+\sigma)^{1/3}\{\ln(1+\sigma)^{1/6}\}$

homo

hetero

$1 / \ln(1+\sigma)$

b

Surface free energy (mJ/m²)
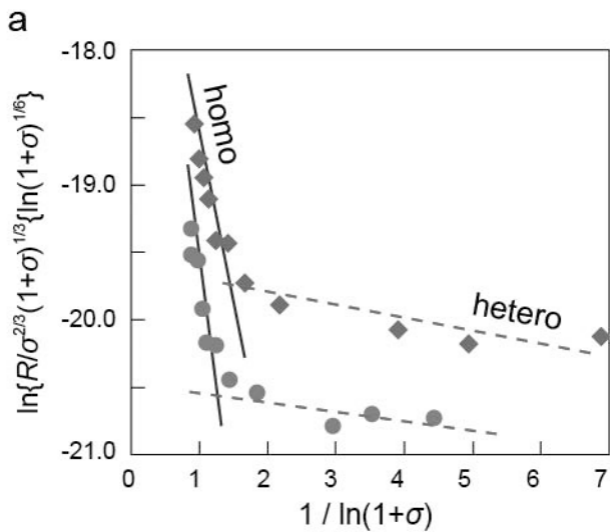
PO_4 concentration (μM)
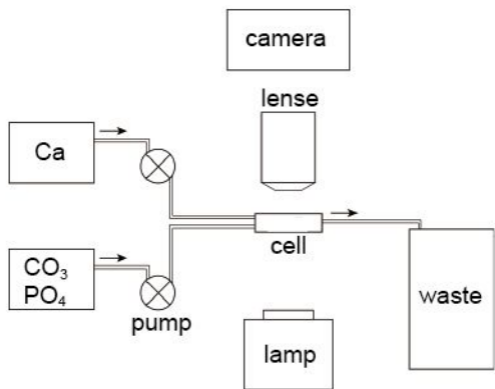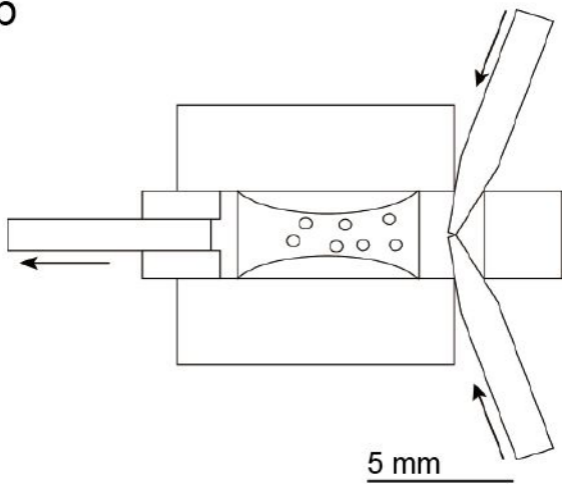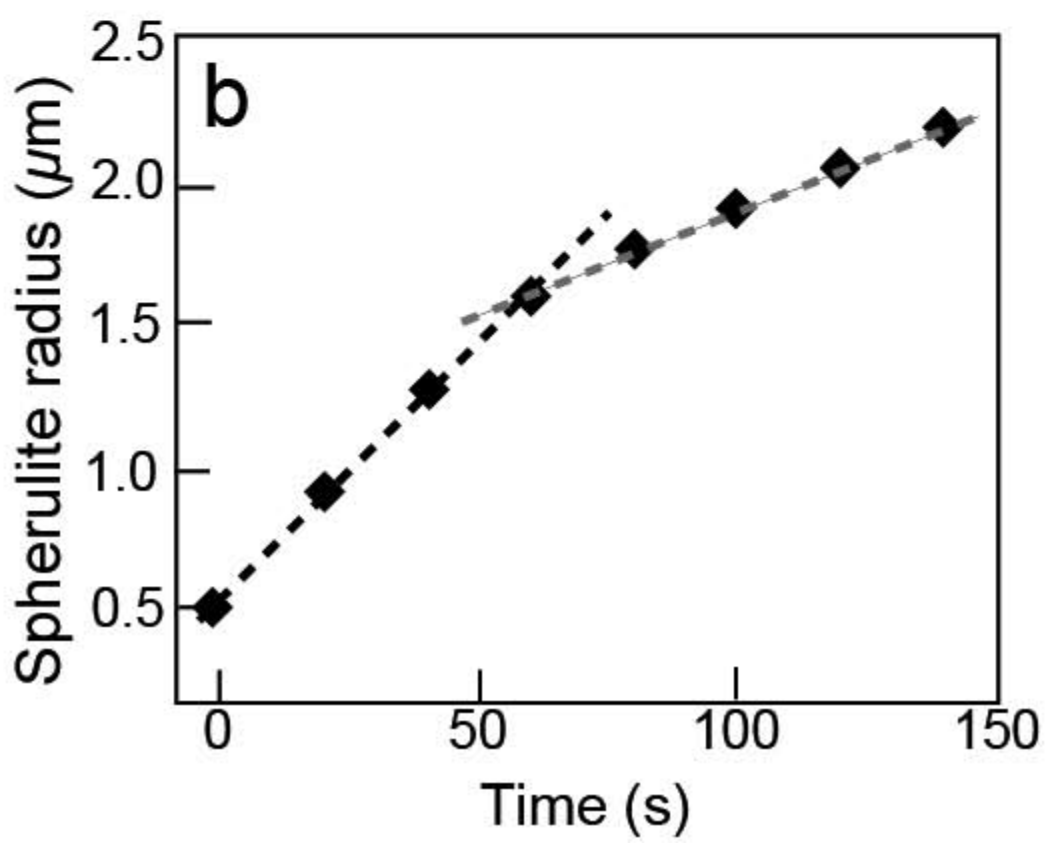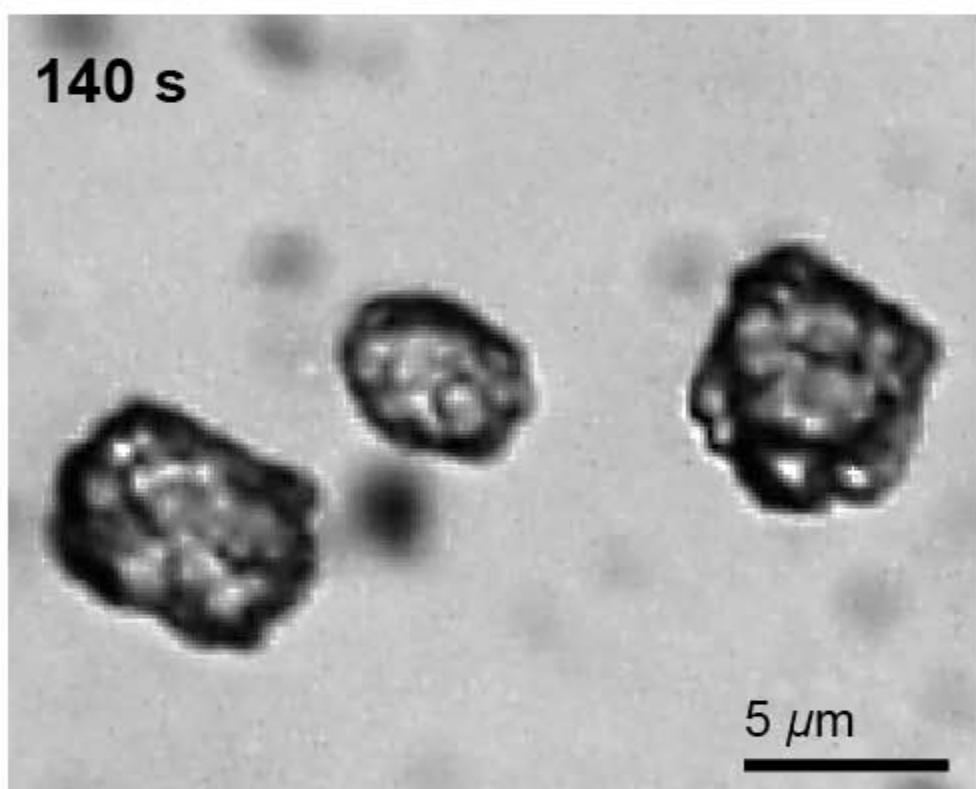
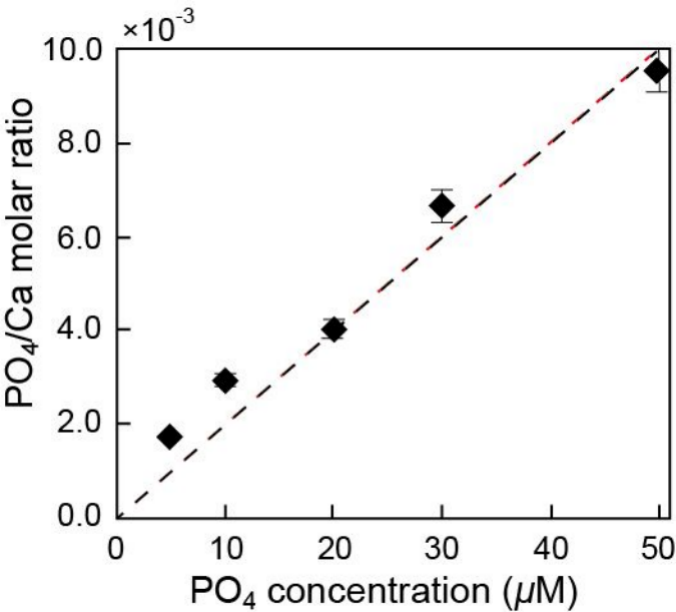|	Vaterite	Pseudo-vaterite
Crystal structure	Highly crystalline phase. Crystallite size was around 200 nm	Low crystalline phase. Crystallite size distribution was bi-modal, around 10 nm and 150 nm.
Chemical composition, C/Ca ratio	1.08 ± 0.08	1.28 ± 0.15
Solubility, Ksp	$Xx*10^{xx}$	$Yy*10^{yy}$
PO4 responce	High response and low absorption	Relatively low response and high absorption